COBEM 2023 27TH INTERNATIONAL CONGRESS OF MECHANICAL ENGINEERING

ABCM Brazilian Society of Mechanical Sciences and Engineering
27th ABCM International Congress of Mechanical Engineering
December 04-08, 2023, Florianópolis-SC, Brazil

COB-2023-1396
NUMERICAL ANALYSIS OF THE THERMOHYDRAULIC PERFORMANCE OF SILVER/WATER NANOFLUIDS IN TURBULENT FLOW

Erick Oliveira do Nascimento
Enio Pedone Bandarra Filho
Federal University of Uberlândia (UFU), School of Mechanical Engineering, Av. Joao Naves de Ávila, 2121-Santa Monica, Uberlândia, MG 38400-902
erick.nascimento@ufu.br
bandarra@ufu.br

Luben Cabezas-Gómez
Heat Transfer Research Group, São Carlos School of Engineering, University of São Paulo, Av. Trabalhador São-Carlense, 400, Pq Arnold Schimidt, CEP 13566-590 – São Carlos, SP, Brazil
lubencg@sc.usp.br

Abstract. *Horizontal tubes are one of the most used heat exchangers in the industry and are usually used in turbulent flows due to the higher heat transfer provided or by the operating characteristic where they are applied. Several researchers have dispersed nanoparticles in conventional coolants in order to increase the thermal conductivity, although this dispersion can also lead to an increase in pumping power, due to the increase in fluid viscosity. Thus, the objective of this work is to numerically evaluate the thermohydraulic performance of silver-water nanofluids in volumetric concentrations of 0.1 – 0.5% in a horizontal circular tube in turbulent flow with inlet temperature of 20 ºC and the specific heat flux of 20 kW/m². The obtained results are compared with experimental and theoretical data available in the literature. From the results obtained, it was identified that the nanofluid with the highest concentration of nanoparticles had an increase of up to 14.23% in the convective coefficient of heat transfer when compared to the base fluid, while the pumping power showed a reduction of up to 3.07% for the same analyzed condition, due to the reduction of up to 5.83% in the Reynolds number due to the increase in dynamic viscosity caused by the addition of nanoparticles. Therefore, all silver-water nanofluids numerically analyzed in this work present better thermohydraulic performance in comparison to the base fluid, making them considered for heat transfer applications in turbulent flow.*

Keywords: *Nanofluid, silver, heat transfer, thermohydraulic performance, computational fluid dynamic*

1. INTRODUCTION

Sarafraz and Hormozi (2015) evaluated the heat transfer and hydraulic behavior of silver/water-ethylene glycol nanofluids in a double pipe heat exchanger. In this analysis, the authors considered laminar, transitional and turbulent flow. For volumetric concentrations of 0.1%, 0.5% and 1%, increases of 22%, 36% and 67% were observed, respectively, in the convective transfer coefficient. Furthermore, increments in the convective heat transfer coefficient tended to be greater in the turbulent regime compared to laminar and transitional flow. This behavior is due to the increase in the Reynolds number, which causes an increase in eddies, intensifying the heat transfer.

Gómez et al. (2017) carried out an experimental study on the thermal and hydraulic performance of nanofluids containing single-walled nanotubes (SWCNT) and silver in distilled water in a straight and horizontal tube. For a constant heat flux, mass flow rates ranging from 30 to 100 g/s and volumetric concentrations of nanoparticles of 0.1%, 0.3% and 0.5%, it was identified that silver nanofluids showed an increase in heat transfer compared to the base fluid, while SWCNT nanofluids showed reduced thermal performance. There was a maximum increase of 1.6%, 3% and 5.5% in the convective heat transfer coefficient when using silver nanofluids with concentrations of 0.1%, 0.3% and 0.5%, respectively.

Al-Rashed et al. (2019) numerically evaluated the thermal and hydraulic behavior of silver/water nanofluids with volumetric concentrations of nanoparticles in the range of 0.1 – 1% in a corrugated microchannel. The results obtained for the base fluid showed satisfactory agreement with the experimental results, with an average difference of 2.88%. The addition of nanoparticles resulted in an increase of up to 24.75% in the convective heat transfer coefficient compared to the base fluid. Additionally, a reduction in pumping power was identified with the increase in the concentration of nanoparticles, resulting in thermohydraulic performance superior to that of the base fluid in all cases analyzed.

Khodabandeh et al. (2020) performed a numerical analysis of heat transfer and pumping power of silver/water nanofluids used as coolants in a spiral heat exchanger, using the two-phase mixture model. For volumetric concentrations of nanoparticles of 2%, 3% and 5%, and a Reynolds number in the range of 500 - 2000, an increase of up to 10.9% in the

overall heat transfer coefficient was verified for the highest concentration of nanoparticles, and at smaller Reynolds number. Additionally, it was identified that the effectiveness factor tends to decrease with an increase in the Reynolds number. When analyzing the ratio between gains in heat transfer and pumping power, it was found that for the concentrations, none of the analyzed nanofluids showed promising results.

Shahsavar et al. (2021) performed an evaluation of the thermohydraulic performance of silver/water nanofluids in laminar flow in a microchannel sink using the Ansys Fluent software. Nanofluids were simulated with volumetric concentrations of 0.1%, 0.5% and 1%, and Reynolds numbers in the range of 500 to 2000. The results showed increases of up to 16.86% and 145% in heat transfer performance with increasing nanoparticle concentration and Reynolds number, respectively. However, the pumping power showed a maximum increase of 8.3% for the highest concentration of nanoparticles, while increasing the Reynolds number resulted in an increase of up to 99.5%. In contrast to the work by Khodabandeh et al. (2020), Shahsavar et al. (2021) identified that the ratio between gains in heat transfer and pumping power for nanofluids was higher than that for the base fluid in most of the analyzed cases.

Kulkarni et al. (2021) prepared silver/water nanofluids with volumetric concentrations in the range of 0.01-0.05% to evaluate their thermal and hydraulic performance in a heat exchanger. It was identified that for the highest volumetric concentration of nanoparticles, the Nusselt number showed an increase of up to 65% compared to the base fluid. When evaluating the thermohydraulic performance, it was identified that in all the analyzed cases, the silver nanofluids presented superior results compared to the base fluid.

Thermal management has broad importance in various applications such as cell phones, aviation, automotive industry, space industry, etc. Furthermore, correct thermal performance allows the reduction of components and increased equipment safety, such as the engine cylinder, fuel cell film and battery thermal runaway, which if not identified, can result in damage to equipment and even human safety. The adoption of nanofluids has the potential to replace conventional fluids, thus achieving high efficiency, energy savings and cost reduction (Lin et al., 2023).

Cieśliński and Kozak (2023) identified in their review work that few studies have conducted a comparative analysis on the application of nanofluids in circular, horizontal and smooth tubes under forced convection. This of analysis can be attributed to the absence of crucial information, such as length, diameter and thickness tube, heat flux, inlet temperature, flow rate/Reynolds number, etc. Therefore, the objective of this work is to contribute to the application of silver/water nanofluids with concentrations of 0.1 - 0.5 vol.% in heat exchangers. The focus is on numerical analysis and comparison with experimental data and theoretical models available in the literature. Turbulent flow conditions are considered in a horizontal, circular and straight pipe, with a constant heat flux of 20 kW/m^2.

2. PHYSICAL MODEL, BOUNDARY CONDITIONS AND GOVERNING EQUATIONS

2.1 Problem geometry and boundary conditions

Figure 1 illustrates the geometry and boundary conditions of the horizontal, circular and straight tube. The wall tube is subjected to a constant heat flux of 20 kW/m^2 and no-slip boundary conditions. The total length of the tube is 2550 mm, with the heated section measuring 2480 mm. The internal and external diameters of the tube are 6.35 mm and 12.7 mm, respectively, which are the same dimensions as those used by Gómez et al. (2017).

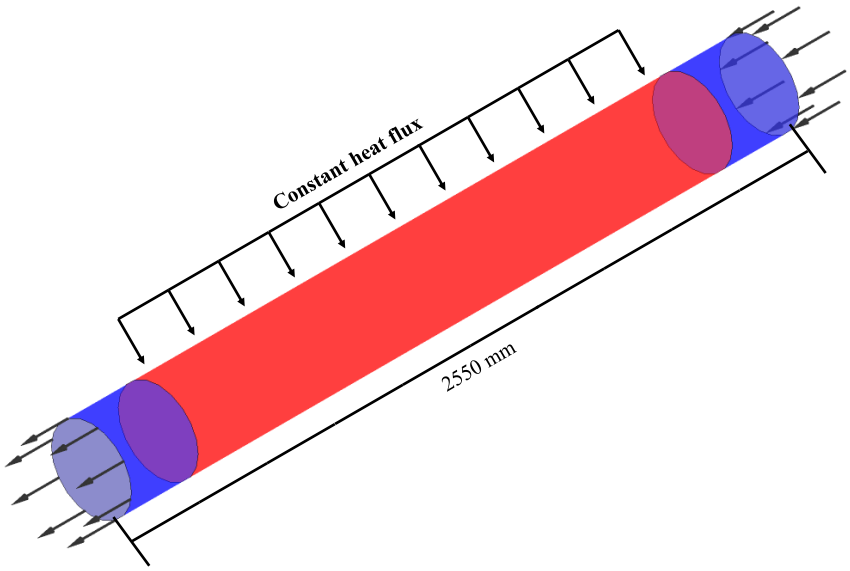

Figure 1. Geometric model and boundary conditions.

The coolant enters the tube at a constant temperature of 20 ºC, and the mass flow rate varies between 30 g/s and 100 g/s, with each mass flow rate being analyzed separately. Additionally, it is assumed that the inner surface of the tube is perfectly smooth, while the outer side is insulated.

2.2 Governing equations

In this work, the assumption is made that the nanofluids are single-phase, meaning that, the silver nanoparticles have the same temperature and velocity as the base fluid. Furthermore, the fluid is considered to be Newtonian and incompressible, with properties dependent on temperature and nanoparticle concentration. Based on these assumptions, the conservation equations for mass, momentum and energy were employed, as described by Eq. (1-3) in the single-phase model, implemented in the Ansys Fluent software.

$$\frac{\partial(\rho u_i)}{\partial x_i} = 0 \tag{1}$$

$$\frac{\partial}{\partial x_i}\left(\rho u_i u_j\right) = -\frac{\partial p}{\partial x_i} + \frac{\partial}{\partial x_j}\left[\mu\left(\frac{\partial u_i}{\partial x_j} + \frac{\partial u_j}{\partial x_i} - \frac{2}{3}\delta_{ij}\frac{\partial u_i}{\partial x_j}\right)\right] + \frac{\partial}{\partial x_j}\left(-\rho\overline{u_i' u_j'}\right) \tag{2}$$

$$\frac{\partial}{\partial x_i}\left[u_i(\rho E + p)\right] = \frac{\partial}{\partial x_i}\left[\left(k + \frac{C_p \mu_t}{Pr_t}\right)\frac{\partial T}{\partial x_j} + u_i\left(\tau_{ij}\right)_{eff}\right] \tag{3}$$

where ρ refers to the fluid density, μ is the dynamic viscosity, C_p denotes the specific heat, k represents the thermal conductivity, p is the fluid pressure, u_i is the component of the velocity vector, x_j is the vector of Cartesian coordinates, u_i' is the component of the instantaneous fluctuation of the velocity, T is the temperature, and δ_{ij} is the Kronecker delta. $E = c_p T - (p/\rho) + (u^2/2)$ is the total energy and $\left(\tau_{ij}\right)_{eff} = \mu\left(\frac{\partial u_j}{\partial x_i} + \frac{\partial u_i}{\partial x_j}\right)$ is the viscous stress tensor.

Due to the flow of the coolant being in the turbulent flow (Reynolds number range of approximately 5665-20051), it was necessary to use a turbulence model to capture the fluctuations of the variables that affect the solution of the problem. The $\kappa - \omega$ SST model was chosen in the simulations because it presents satisfactory results in problems like the one analyzed in this work, as identified by Sadri et al. (2018). Furthermore, the $\kappa - \omega$ SST model is not excessively sensitive to boundary conditions (Fluent, 2013). The turbulent kinetic energy rate (κ) and the specific dissipation rate (ω) are defined through Eq. (4) and Eq. (5), respectively. More details of the $\kappa - \omega$ SST turbulence model can be found in Fluent (2013).

$$\frac{\partial}{\partial x_i}(\rho\kappa u_i) = \frac{\partial}{\partial x_j}\left(\Gamma_\kappa \frac{\partial \kappa}{\partial x_j}\right) + \tilde{G}_\kappa - Y_\kappa + S_\kappa \tag{4}$$

$$\frac{\partial}{\partial x_i}(\rho\omega\kappa u_i) = \frac{\partial}{\partial x_j}\left(\Gamma_\omega \frac{\partial \omega}{\partial x_j}\right) + G_\omega - Y_\omega + D_\omega + S_\omega \tag{5}$$

2.3 Numerical method

The differential equations were discretized using the Finite Volume Method (FVM) employing the Semi-Implicit Method for Pressure Linked Equations (SIMPLE) pressure-velocity coupling scheme. To discretize the diffusive and convective terms, the second-order upwind scheme was utilized (Fluent, 2013). For convergence criteria, it was specified that the residuals should be less than 10^{-6}, except for the energy equation, where a value of 10^{-9} was employed.

2.4 Thermophysical properties of the coolants

The thermophysical properties of the coolants used in this work for the inlet temperature are presented in Table 1. It is important to note that the properties of the fluids depend on the volumetric concentration of the silver nanoparticle and the local temperature of the flow. This consideration adds realism to the temperature, pressure and velocity fields. To account for this, a User-Defined Function (UDF) was implemented in the Ansys Fluent software for each property, considering the temperature and volumetric concentration of the nanoparticle. According to Safaei et al. (2016), this approach is recommended to minimize errors associated with the single-phase approach.

Silver nanoparticles are spherical and obtained in powder, whose geometric specification and properties were provided by Nanostructures & Amorphous Material Inc. and are described in the work of Gómez et al. (2017).

Table 1. Thermophysical properties of the water and silver aqueous nanofluids at an inlet temperature of 20 °C.

Properties\ Coolant	**Base fluid**	**0.1 vol.%**	**0.3 vol.%**	**0.5 vol.%**
Thermal Conductivity [W/m·K]	0.586	0.630	0.689	0.794
Specific Heat [J/kg·K]	4183.74	4142.55	4062.46	3985.28
Density [kg/m^3]	998.37	1007.87	1026.88	1045.88
Dynamic Viscosity [Pa·s]	0.00099998	0.00101552	0.00103882	0.00106189

Source: Gómez et al. (2017).

The thermal conductivity (k) and dynamic viscosity (μ) values were obtained from the work by Gómez et al. (2017). The density (ρ) and specific heat (C_p) of the base fluid were obtained from the Engineering Equation Solver (EES) software database. The calculations for the nanofluids were performed using the models proposed by Pak and Cho (1998) (Eq. (6)) and Xuan and Rotzel (2000) (Eq. (7)), as applied by Gómez et al. (2017).

$$\rho_{nf} = (1 - \emptyset)\rho_{bf} + \emptyset\rho_{np} \tag{6}$$

$$C_{p,nf} = \frac{(1 - \emptyset)\rho_{bf}C_{p,bf} + \emptyset\rho_{np}C_{p,np}}{(1 - \emptyset)\rho_{bf} + \emptyset\rho_{np}} \tag{7}$$

where ∅ represents the volumetric concentration of the nanoparticle. The subscripts np, bf and nf, refer to the nanoparticle, base fluid and nanofluid, respectively.

2.5 Data reduction

To obtain the parameters analyzed in this work and compare them, the same equations by Gómez et al. (2017) were used. The local convective heat transfer coefficient (h was obtained using Eq. (8).

$$h = \frac{q''}{\left(T_{W(z)} - T_{m(z)}\right)} \tag{8}$$

where q'' refers to the heat flux and $T_{W(z)}$ and $T_{m(z)}$ represent the wall and fluid temperature, respectively, in the flow direction.

The average convective heat transfer coefficient consists of an average of the local values, according to Eq. (9).

$$h_{avg} = \frac{h(z_1) + \cdots + h(z_n)}{n} \tag{9}$$

To compare and validate the thermal and hydraulic results obtained for the base fluid, the correlations of Gnielinski (1975) and Petukhov (1970) were used to calculate the Nusselt number (*Nu*) and the theoretical friction factor (*f*) through Eq. (10) and Eq. (11), respectively.

$$Nu = \frac{\frac{f}{8}(Re - 1000)Pr}{1 + 12.7 \cdot \left(\frac{f}{8}\right)^{1/2}(Pr^{2/3} - 1)} \tag{10}$$

$$f = (0.79ln(Re) - 1.64)^{-2} \tag{11}$$

where *Re* represents the Reynolds number and *Pr* refers to the Prandtl number.

The values obtained in Eq. (10) and Eq. (11) were used in Eq. (12) and Eq. (13), respectively, to calculate the theoretical average convective heat transfer coefficient and pressure drop.

$$Nu_{avg}\frac{h_{avg} \cdot D}{k} \tag{12}$$

$$f = \frac{\Delta p\rho\pi^2 D^5}{8L\dot{m}^2} \tag{13}$$

where D refers to the hydraulic diameter of the tube, L is the length of the tube, Δp is the pressure drop, and k and ρ refer to the thermal conductivity and density of the coolant, respectively.

For the analysis of the thermohydraulic performance (numerical, experimental, and theoretical) of the nanofluids, Eq. (14) was utilized.

$$\eta = \frac{h_{avg,nf}/h_{avg,bf}}{\Delta p_{nf}/\Delta p_{bf}} \tag{14}$$

3. RESULTS AND DISCUSSIONS

As performed by Gómez et al. (2017), in the present work, the coolants were analyzed in a horizontal tube with constant inlet temperature at 20 ºC and mass flow rate ranging from 30 g/s to 100 g/s (Reynolds number between 5665 and 20051). Additionally, a constant heat flux of 20 kW/m^2 was applied to the tube wall. The thermal and hydraulic results are then compared with the values obtained by Gómez et al. (2017) and calculated using the correlations described earlier.

3.1 Grid independence study

In order to ensure that the results were independent of element size, a mesh independence study was conducted for three different element sizes. Table 2 presents the number of elements, the convective coefficient of heat transfer of the base fluid, and the difference compared to the experimental result of Gómez et al. (2017). The structured mesh was generated using a package provided by the Ansys Fluent software. The meshes used in this work have 15 layers of prismatic elements with a growth rate of 1.2 in the regions near to the wall, to capture the large velocity and temperature gradients (Sadri et al., 2018).

Table 2. Grid independence study and comparison with the experimental result by Gómez et al. (2017).

Mesh\Parameter	Number of elements	h_{avg} [W/m·K]	Difference [%]	$\Delta p/L$[kPa/m]	Difference [%]
1	67096	15165.27	10.56	21.85	4.68%
2	91506	14064.71	2.54	21.67	3.83%
3	122310	13997.31	2.05	21.66	3.77%

It was identified that the mesh with 91506 elements provides satisfactory results for the convective heat transfer coefficient and the pressure drop. The differences found are like what was obtained by Shahsavar et al. (2022). Increasing the number of elements increases the computational cost and does not significantly influence the result. From these considerations, the mesh with 91506 elements was selected for the simulations.

3.2 Validation

The validation of the numerically obtained thermal and hydraulic results was performed for the base fluid using experimental results from Gómez et al. (2017) and theoretical correlations (Gnielinski, 1975 and Petukhov, 1970). In this procedure, the average convective heat transfer coefficient and the pressure drop values were compared, as shown in Figures 2 and 3, respectively. The numerically obtained results demonstrate satisfactory agreement, the experimental results of Gómez et al. (2017), with average differences of 3.76% for the convective heat transfer coefficient and 14.10% for the pressure drop.

It should be noted that these differences can be attributed to the omission of conduction resistance in the test section, as not considered in the numerical model (Sadri et al., 2018). Additionally, errors associated with approximations made by the turbulence model can also contribute to these discrepancies. However, it is worth mentioning that all average convective heat transfer coefficient values are in the uncertainty range, expect for the mass flow rate of 30 g/s. Based on the forementioned, it can be concluded that the numerical model adequately simulates the thermal and hydraulic behavior of the coolant.

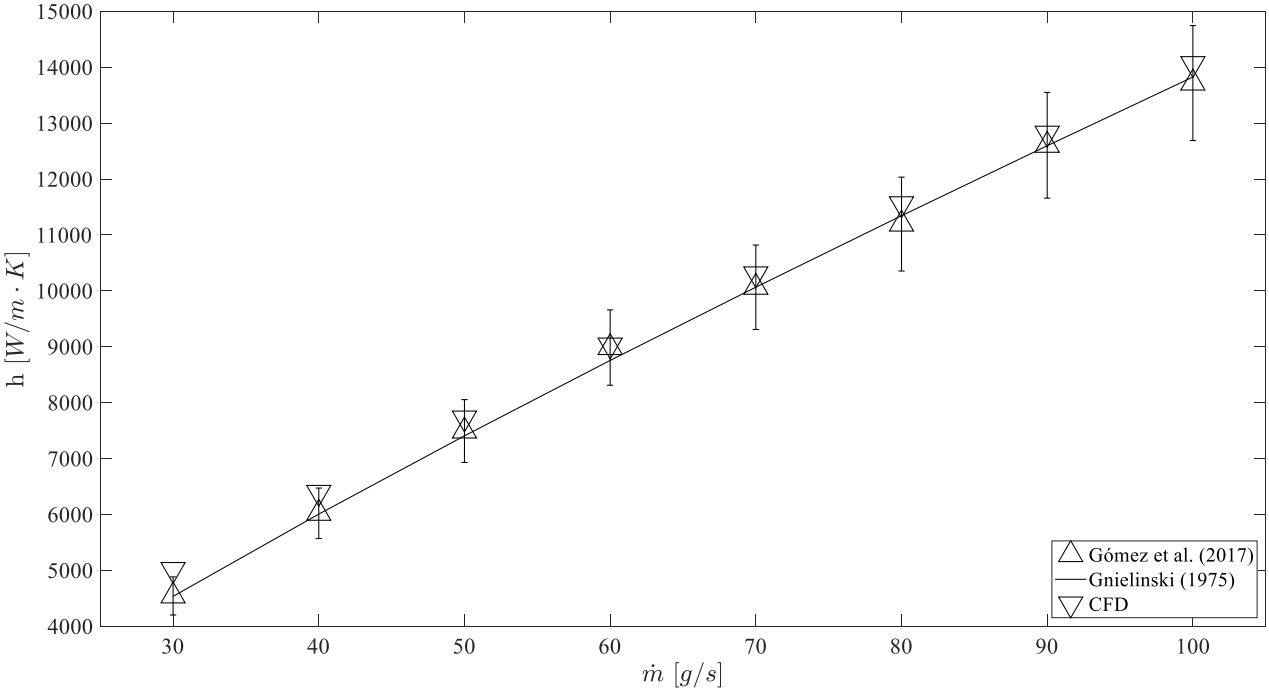

Figure 2. Comparison of average convective heat transfer coefficient for the base fluid (experimental, theoretical, and numerical).

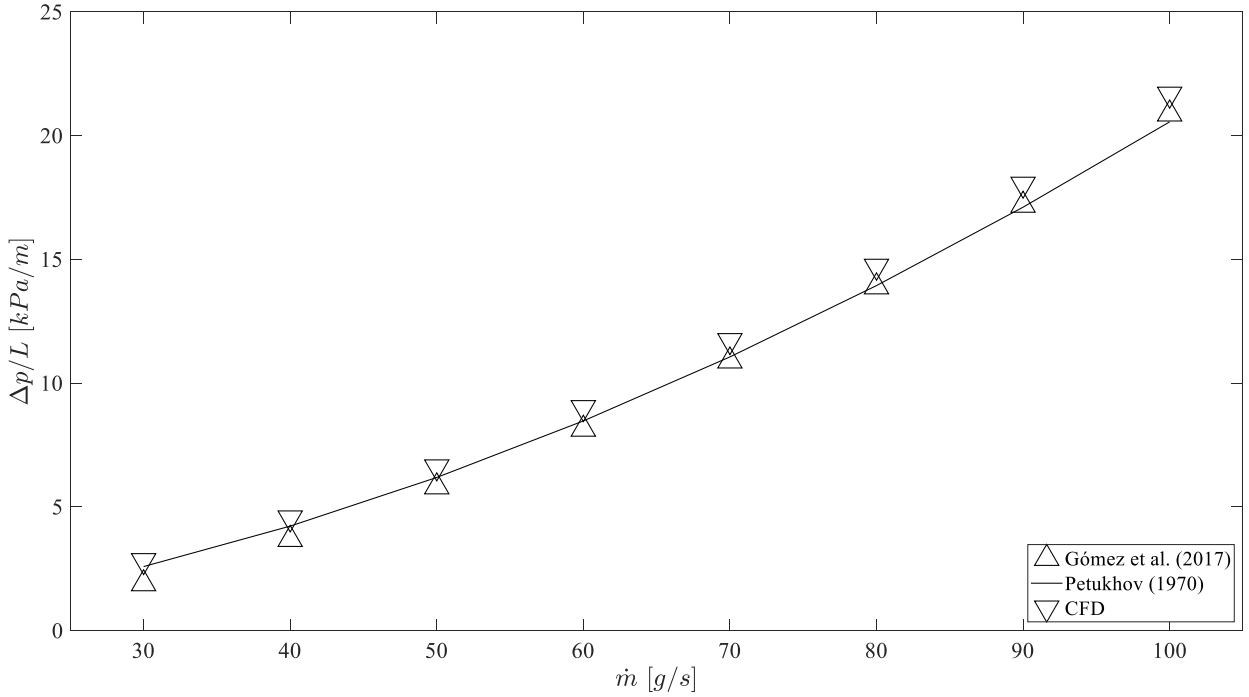

Figure 3. Comparison of pressure drop for the base fluid (experimental, theoretical, and numerical).

3.3 Heat transfer coefficient

In Table 3 and in Figure 4 shows the results of the average convective heat transfer coefficient obtained experimentally by Gómez et al. (2017) and those reached numerically in this work. It was identified that the results obtained numerically present satisfactory agreement with the experimental results, however, the increase in the volumetric concentration of silver nanoparticles increased the differences in the obtained values. The average differences were 3.76%, 5.59%, 8.06% and 12.49% for the base fluid and the nanofluids with the volumetric concentrations of 0.1%, 0.3% and 0.5%, respectively. The differences between the two methodologies (experimental and numerical) for the base fluid, is like that found by

Sadri et al. (2018) and Al-Rashed et al. (2019). The differences found with the increase in the volumetric concentration of silver nanoparticles can be explained by the high concentration of nanoparticles, which tend to increase abruptly phenomena such as the Brownian motion of the particles, which disturbs the thermal boundary layer resulting in more particle-particle collision causing greater chances of agglomeration of nanoparticles mainly for volumetric concentration of 0.5% (Chakraborty and Panigrahi, 2020).

Table 3. Numerical average convective heat transfer coefficient and comparison with the experimental result by Gómez et al. (2017).

Author\ Mass flow rate	**100 [g/s]**	**90 [g/s]**	**80 [g/s]**	**70 [g/s]**	**60 [g/s]**	**50 [g/s]**	**40 [g/s]**	**30 [g/s]**
Present work – Base fluid	14064.71 [W/m·K]	12820.52 [W/m·K]	11558.19 [W/m·K]	10303.97 [W/m·K]	9030.88 [W/m·K]	7725.37 [W/m·K]	6395.66 [W/m·K]	5015.68 [W/m·K]
Gómez et al. (2017) – Base fluid	13716.80 [W/m·K]	12603.70 [W/m·K]	11194.40 [W/m·K]	10064.80 [W/m·K]	8985.70 [W/m·K]	7492.90 [W/m·K]	6021.40 [W/m·K]	4543.10 [W/m·K]
Difference	2.54%	1.72%	3.25%	2.38%	0.50%	3.10%	6.22%	10.40%
Present work – 0.1 vol.%	14523.02 [W/m·K]	13232.99 [W/m·K]	11935.85 [W/m·K]	10647.51 [W/m·K]	9332.17 [W/m·K]	7988.02 [W/m·K]	6612.4 [W/m·K]	5188.92 W/m·K
Gómez et al. (2017) – 0.1 vol.%	13943.30 W/m·K	12841.00 W/m·K	11539.20 W/m·K	10263.6 [W/m·K]	8936.50 [W/m·K]	7466.70 [W/m·K]	6161.00 [W/m·K]	4649.50 [W/m·K]
Difference [%]	4.16%	3.05%	3.44%	3.74%	4.43%	6.98%	7.33%	11.60%
Present work – 0.3 vol.%	15016.44 [W/m·K]	13685.75 [W/m·K]	12352.36 [W/m·K]	11029.17 [W/m·K]	9664.76 [W/m·K]	8280.73 [W/m·K]	6855.49 [W/m·K]	5382.15 [W/m·K]
Gómez et al. (2017) – 0.3 vol.%	14101.10 [W/m·K]	12917.70 [W/m·K]	11736.20 [W/m·K]	10341.50 [W/m·K]	9050.10 [W/m·K]	7660.90 [W/m·K]	6205.60 [W/m·K]	4688.30 [W/m·K]
Difference	6.49%	5.95%	5.25%	6.65%	6.79%	8.09%	10.47%	14.80%
Present work – 0.5 vol.%	15990.43 [W/m·K]	14578.62 [W/m·K]	13168.74 [W/m·K]	11775.99 [W/m·K]	10317.28 [W/m·K]	8849.58 [W/m·K]	7330.05 [W/m·K]	5759.35 [W/m·K]
Gómez et al. (2017) – 0.5 vol.%	14525.30 [W/m·K]	13368.10 [W/m·K]	12014.80 [W/m·K]	10738.20 [W/m·K]	9308.30 [W/m·K]	7789.00 [W/m·K]	6288.20 [W/m·K]	4778.60 [W/m·K]
Difference	10.09%	9.06%	9.60%	9.66%	10.84%	13.62%	16.57%	20.52%

Gómez et al. (2017) reported increases in the average convective heat transfer coefficient of 1.6%, 3% and 5.5% for samples with volumetric concentrations of 0.1%, 0.3% and 0.5%, respectively. In contrast, the present work observed average gains of 3.33%, 7.02% and 14.23% for the same nanofluids. The smaller increase in the average convective heat transfer coefficient in the experimental methodology can be attributed to the probable agglomeration of nanoparticles, which tends to decrease heat transfer and other phenomena occurring in a colloidal suspension, not accounted for in the simulations. Moreover, agglomeration tends to increase dynamic viscosity, potentially increasing the thickness of the thermal boundary layer and reducing heat transfer and increasing the pressure drop (Huang et al., 2015). The increases in dynamic viscosity are so significant for concentrations above 0.1 vol.% that Selvam et al. (2016) recommended limiting use of silver nanofluids to concentrations up to 0.15 vol.%. These results suggest that the two-phase approach should be investigated for silver/water nanofluid applications with concentrations greater than 0.1 vol.% to incorporate these phenomena and compare the results with the single-phase approach.

As shown in Figure 4, the numerically obtained average convective heat transfer coefficient shows an increase as a function of mass flow rate, exhibiting a linear behavior (for both the base fluid and the nanofluid) within the analyzed mass flow rate range, consistent with the findings of Gómez et al. (2017). In all numerically analyzed cases, the h_{avg}

increased with the concentration of nanoparticles. Furthermore, the gains in the convective coefficient with the addition of nanoparticles are relatively almost constant as the mass flow rate increased.

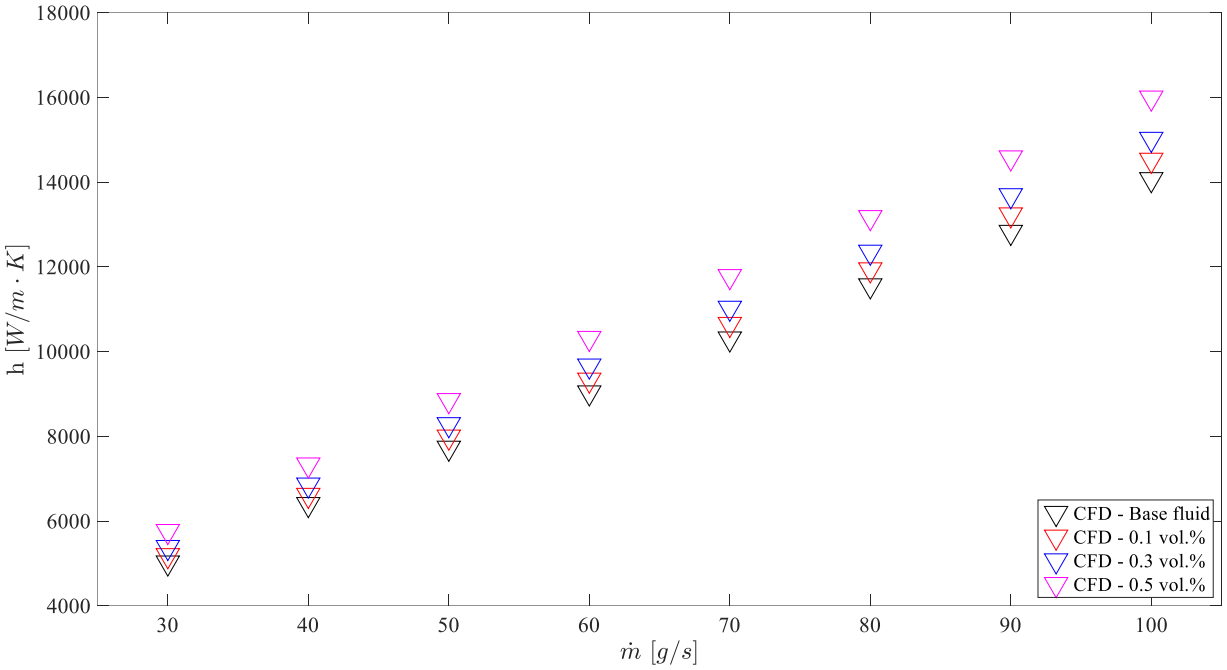

Figure 4. Numerical average convective heat transfer coefficient as a function of a mass flow rate.

3.4 Pressure drop

In Figure 5, the pressure drop per unit length obtained numerically is illustrated. A decrease of up to 3.06% in the pressure drop was identified as a function of the increase in the volumetric concentration of nanoparticles. This behavior can be explained by considering a constant mass flow rate and the increase in dynamic viscosity with the addition of nanoparticles, which tends to decrease the Reynolds number (by up to 5.83%) and, consequently the pressure drop, as observed by Al-Rashed et al. (2019), Naveen and Kishore (2020) and Bai et al. (2020). Additionally, as expected, there was an increase in pressure drop with an increasing mass flow rate, as also observed by Gómez et al. (2017).

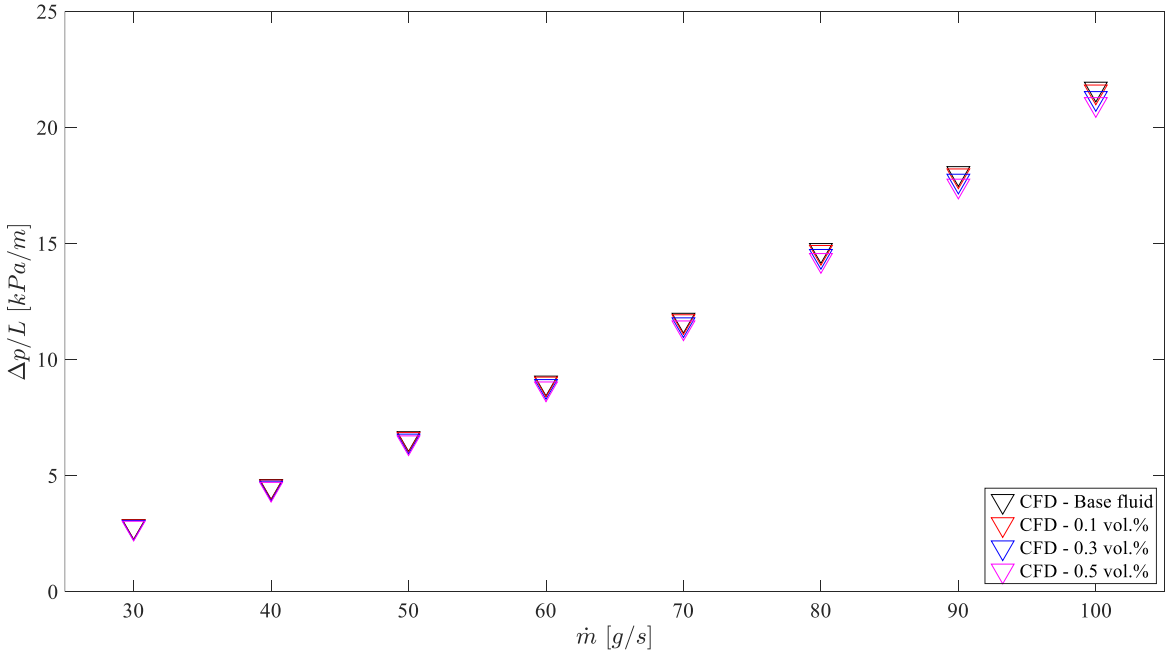

Figure 5. Numerical pressure drop as a function of a mass flow rate.

3.5 Thermohydraulic performance

Figure 6 illustrates the thermohydraulic performance of the coolants obtained numerically in this work, experimentally by Gómez et al. (2017), and through theoretical models for single-phase flow. It was found that the numerical model shows better agreement for concentrations up to 0.1 vol.%. For the concentration of 0.3 vol.%, both the theoretical and numerical models are consistent with each other, but they deviate from the experimental results. For the concentration of 0.5 vol.%, all three models exhibit discrepancies among themselves, which can be attributed to phenomena occurring in the flow and heat transfer of nanofluids, that are not considered in the simulations or theoretical models. These phenomena include agglomeration, sedimentation, Brownian motion, diffusiophoresis, etc., which directly affect the heat transfer and pressure drop of nanofluids (Guo, 2020). According to Koo and Kleinstreuer (2005), the interaction between particles cannot be neglected for volumetric concentrations of 0.5%, making it necessary to use a two-phase model to capture these phenomena.

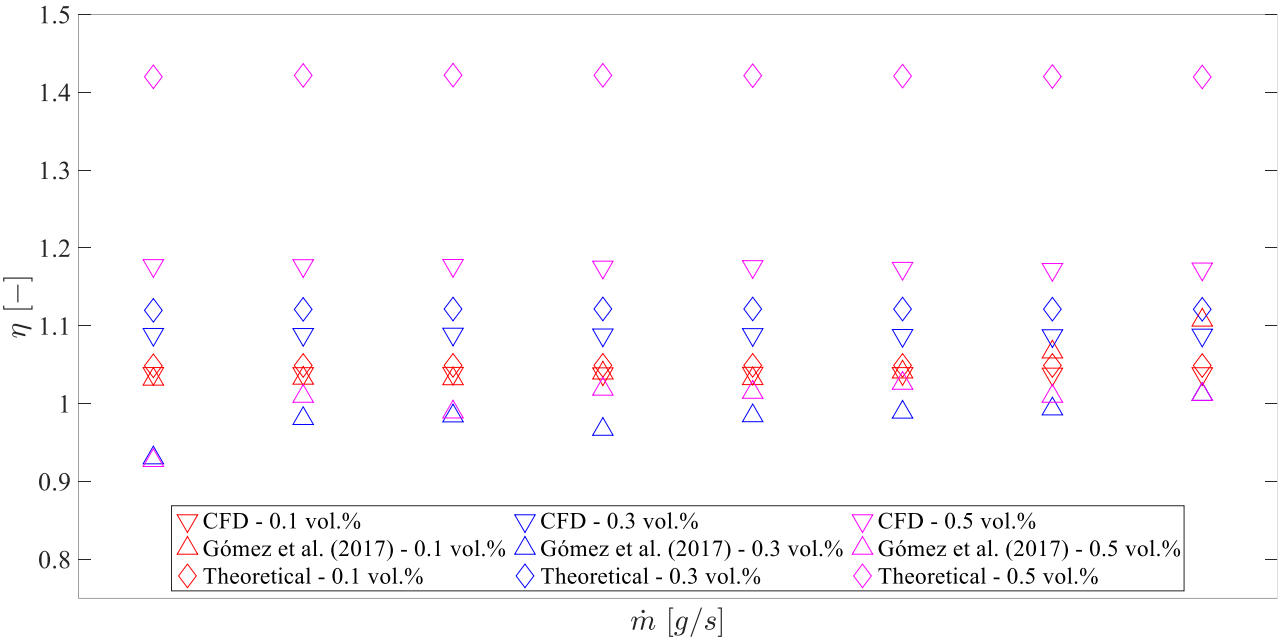

Figure 6. Comparison of thermohydraulic performance (experimental, theoretical, and numerical).

For volumetric concentrations of 0.3% and 0.5%, both the theoretical models and the numerical modeling show higher thermohydraulic performance (η) than the experimental results, and this performance tends to increase with the increase in nanoparticle concentration of nanoparticles. However, in the experimental study conducted by Gómez et al. (2017), higher η values were observed for the lowest concentration. Additionally, it was identified that the numerically analyzed nanofluids exhibit superior thermohydraulic performance compared to the base fluid in all analyzed cases, as reported by Al-Rashed et al. (2019) on the application of silver-water nanofluids in a heat sink.

4. CONCLUSIONS

In the present work, a numerical and comparative study of the thermohydraulic performance of silver/water nanofluids in a straight, horizontal and circular tube was presented. The effects of varying the volumetric concentration of nanoparticles in the range of 0.1% to 0.5% and the mass flow rate from 30 g/s to 100 g/s in a turbulent flow were investigated, under a constant heat flux of 20 kW/m^2. The numerical model successfully predicts the thermohydraulic behavior of the analyzed coolants in this work up to a concentration of 0.1 vol.%. For higher concentrations, both the numerical and theoretical models tend to yield values higher than the experimental results, due to simplifications in the approaches that neglect certain phenomena influencing heat transfer and pressure drop. The numerical results indicate enhancements in thermohydraulic performance of up to 3.85%, 8.83% and 11.75% for nanofluids with volumetric concentrations of 0.1%, 0.3% and 0.5%, respectively. Additionally, the use of the two-phase model is recommended to predict the thermal and hydraulic behavior of silver nanofluids and compare it with the single-phase approach and the experimental results.

5. ACKNOWLEDGEMENTS

The authors are grateful for the financial support provided for this research by CAPES, CNPq and FAPEMIG.

6. REFERENCES

Al-rashed, A.A.A.A.; Shahsavar, A.; Rasooli, O.; Moghimi, M.A.; Karimipour, A.; Tran, M.D., 2019. Numerical assessment into the hydrothermal and entropy generation characteristics of biological water-silver nano-fluid in a wavy walled microchannel heat sink. International Communications in Heat and Mass Transfer, v. 104, p. 118-126.

Bai, M.; Liu, J.; He, J.; Li, W.; Wei, J.; Chen, L.; Miao, J.; Li, C., 2020. Heat transfer and mechanical friction reduction properties of graphene oxide nanofluids. Diamond and Related Materials, v. 108, p. 107982.

Chakraborty, S.; Panigrahi, P.K., 2020. Stability of nanofluid: a review. Applied Thermal Engineering, v. 174, p. 115259.

Cieśliński, J.T.; Kozak, P., 2023. Experimental investigations of forced convection of nanofluids in smooth, horizontal, round tubes: a review. Energies, v. 16, n. 11, p. 4415.

Fluent, A., 2013. Ansys Fluent Theory Guide. ANSYS Inc., USA, v. 15317, p. 724-46.

Gnielinski, V., 1975. Neue gleichungen für den wärme- und den stoffübergang in turbulent durchströmten rohren und kanälen. Forschung Im Ingenieurwesen, v. 41, n. 1, p. 8-16.

Gómez, A.O.C.; Alegrias, J.G.P.; Bandarra Filho, E.P., 2017. Experimental analysis of the thermal-hydraulic performance of water based silver and SWCNT nanofluids in single-phase flow. Applied Thermal Engineering, v. 124, p. 1176-1188.

Guo, Z., 2020. A review on heat transfer enhancement with nanofluids. Journal of Enhanced Heat Transfer, p. 1-70.

Huang, D.; Wu, Z.; Sunden, B., 2015. Pressure drop and convective heat transfer of Al_2O_3/water and MWCNT/water nanofluids in a chevron plate heat exchanger. International Journal of Heat and Mass Transfer, v. 89, p. 620-626.

Khodabandeh, E.; Boushehri, R.; Akbari, O.A.; Akbari, S.; Toghraie, D., 2020. Numerical investigation of heat and mass transfer of water—silver nanofluid in a spiral heat exchanger using a two-phase mixture method. Journal of Thermal Analysis and Calorimetry, v. 144, n. 3, p. 1003-1012.

Lin, H.; Jian, Q.; Bai, X.; Li, D.; Huang, Z.; Huang, W.; Feng, S.; Cheng, Z., 2023. Recent advances in thermal conductivity and thermal applications of graphene and its derivatives nanofluids. Applied Thermal Engineering, v. 218, p. 119176.

Naveen, N.S.; Kishore, P.S., 2020. Experimental investigation on heat transfer parameters of an automotive car radiator using graphene/water-ethylene glycol coolant. Journal of Dispersion Science and Technology, v. 43, p. 1-13.

Pak, B.C.; Cho, Y.I., 1998. Hydrodynamic and heat transfer study of dispersed fluids with submicron metallic oxide particles. Experimental Heat Transfer, v. 11, n. 2, p. 151-170.

Petukhov, B.S., 1970. Heat transfer and friction in turbulent pipe flow with variable physical properties. Advances in Heat Transfer, p. 503-564.

Koo, J.; Kleinstreuer, C., 2005 Impact analysis of nanoparticle motion mechanisms on the thermal conductivity of nanofluids. International Communications in Heat and Mass Transfer, v. 32, n. 9, p. 1111-1118.

Kulkarni, H. R.; Dhanasekaran, C.; Rathnakumar, P.; Sivaganesan, S., 2021. Experimental study on thermal analysis of helical coil heat exchanger using green synthesis silver nanofluid. Materials Today: Proceedings, v. 42, p. 1037-1042.

Sadri, R.; Mallah, A.R.; Hosseini, M.; Ahmadi, G.; Kazi, S.N.; Dabbagh, A.; Yeong, C.H.; Ahmad, R.; Yaakup, N.A., 2018. CFD modeling of turbulent convection heat transfer of nanofluids containing green functionalized graphene nanoplatelets flowing in a horizontal tube: comparison with experimental data. Journal of Molecular Liquids, p. 152-159.

Safaei, M.R.; Jahanbin, A.; Kianifar, A.; Gharehkhani, S.; Kherbeet, A.S.; Goodarzi, M.; Dahari, M., 2016. Mathematical modeling for nanofluids simulation: a review of the latest works. Modeling and Simulation in Engineering Sciences.

Sarafraz, M.M.; Hormozi, F., 2015 Intensification of forced convection heat transfer using biological nanofluid in a double-pipe heat exchanger. Experimental Thermal and Fluid Science, v. 66, p. 279-289.

Selvam, C.; Irshad, E.C. Muhammed; Lal, D. Mohan; Harish, Sivasankaran., 2016. Convective heat transfer characteristics of water–ethylene glycol mixture with silver nanoparticles. Experimental Thermal and Fluid Science, v. 77, p. 188-196.

Shahsavar, A.; Alimohammadi, S.; Askari, I.B.; Shahmohammadi, M.; Jamei, M.; Pouyan, N., 2022. Two-phase mixture numerical and soft computing-based simulation of forced convection of biologically prepared water-silver nanofluid inside a double-pipe heat exchanger with converging sinusoidal wall: hydrothermal performance and entropy generation analysis. Engineering Analysis with Boundary Elements, v. 143, p. 43-60.

Shahsavar, A.; Entezari, S.; Askari, I.B.; Ali, H.M., 2021. The effect of using connecting holes on heat transfer and entropy generation behaviors in a micro channels heat sink cooled with biological silver/water nanofluid. International Communications in Heat and Mass Transfer, v. 123, p. 104929.

Xuan, Y.; Roetzel, W., 2000. Conceptions for heat transfer correlation of nanofluids. International Journal of Heat and Mass Transfer, v. 43, n. 19, p. 3701-3707.

7. RESPONSIBILITY NOTICE

The author(s) is (are) the only responsible for the printed material included in this paper.